HNPS Advances in Nuclear Physics

Vol 13 (2004)

HNPS2004

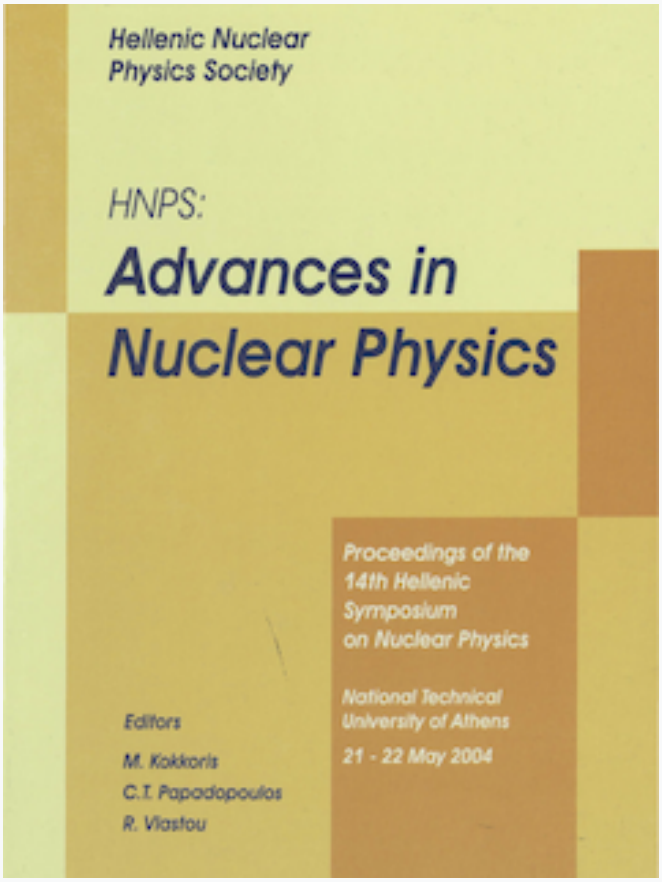

Realistic Calculations for Cold Dark Matter Detection Rates

T. S. Kosmas, M. Kortelainen, J. Suhonen, J. Toivanen

doi: 10.12681/hnps.2978

Realistic Calculations for Cold Dark Matter Detection Rates

T. S. Kosmas [a], M. Kortelainen [b] J. Suhonen [b] J. Toivanen [b]

[a] *Theoretical Physics Division, University of Ioannina, GR-45110 Ioannina, Greece*

[b] *Department of Physics, University of Jyväskylä, P.O.Box 35, FIN-40351, Jyväskylä, Finland*

Abstract

The scattering of the cold dark matter (CDM) candidate LSP (Lightest Supersymmetric Particle) off nuclei is investigated. We focus on the nuclear-structure aspects of the LSP-nucleus scattering problem and computed the associated event rates as well as the annual modulation signals for the ^{23}Na, ^{71}Ga, ^{73}Ge and ^{127}I CDM detectors by using the nuclear shell model in realistic model spaces and exploiting microscopic effective two-body interactions. Large-scale computations had to be performed in order to achieve convergence of the results. The relevance of the spin-dependent and coherent channels for the event rates is discussed, from both the nuclear structure and the SUSY-model viewpoints.

1 Introduction

The recent combined observations of stars and galaxies over a large range of scales indicate that most of the matter in the Universe is dark (seen only through its gravitational effects) and that much of this dark matter is non-baryonic and cold (CDM) [1–4]. On the theoretical side, recent supersymmetric (SUSY) models rather generically provide well motivated CDM candidates for weakly-interacting massive particles (WIMPs) which, if they exist, would make up a major component of the dark matter in our own galactic halo [2,3].

Up to now, important efforts have been undertaken by several groups in terrestrial searches of cold dark matter [4–8] in order to test a large sample of the SUSY parameter space. To this aim, direct detection experiments appear as one of the most promising techniques to detect WIMPs of our galaxy by looking for the interaction of WIMPs with target nuclei, e.g. by recording the recoil energy of nuclear targets as WIMPs scatter off them. The first direct

detection experiment, DAMA [4], uses high-purity NaI crystals. Despite the fact that NaI is inefficient in discrimination at low energies the DAMA has reported the first indication of an annual modulation signal.

Much progress related to background discrimination capabilities was achieved by other direct detection experiments developed successfully over the last decade [4–10]. Thus, in the gryogenic experiments, CDMS (with Ge and Si detectors) [5], EDELWEISS (with a ^{73}Ge target) [6], CRESST [7] and ROSEBUD [8], the detectors are capable of detecting simultaneously two signals. For the CDMS and EDELWEISS these are the ionization and phonon signals whereas for the CRESST and ROSEBUD the scintillation and phonon signals are detected. We also mention that the ZEPLIN collaboration [2,9] has developed a liquid Xe detector with a discrimination based on the diffent scintillation-time constants for nuclear and electron recoils.

Over the next 2-3 years [2,11] the direct CDM detection experiments plan to improve their present sensitivity by nearly one to two orders of magnitude (i.e. to less than one interaction per kilogram and per year) which will allow to test a much larger fraction of the realistic SUSY models. This will require large detector mass, low energy thresholds, efficient nuclear recoil detection and long counting times on the experimental side and detailed LSP-nucleus cross section calculations on the theory side.

The main purpose of the present Letter is to focus on the key ingredients in the calculation of the signal in direct detection experiments by using reliable nuclear-structure methods. Our calculated results enable prediction of event rates (per unit time and unit of detector mass) for the above-mentioned experiments. The considered scattering processes involve two main classes of couplings: spin-dependent (axial-vector) interactions and spin-independent (scalar scattering) ones.

In the present Letter we will assume the WIMP candidate for the CDM to be the Lightest Supersymmetric Particle (LSP). As it is well known, in the framework of the minimal supersymmetric standard model (MSSM) the superpartners bino ($\tilde{B}$), wino ($\tilde{W}_3$) and the two higgsinos ($\tilde{H}_1^0$, $\tilde{H}_2^0$) mix to form four Majorana mass eigestates called neutralinos. They are usually denoted as $\tilde{\chi}_1^0, \tilde{\chi}_2^0, \tilde{\chi}_3^0, \tilde{\chi}_4^0$, with increasing mass. The LSP is the lightest neutralino, i.e. a linear combination of the type $\chi \equiv \tilde{\chi}_1^0 = c_{11}\tilde{B} + c_{12}\tilde{W}_3 + c_{13}\tilde{H}_1^0 + c_{14}\tilde{H}_2^0$, with $c_{1j}, j = 1,2,3,4$, representing the mixing parameters [3,12]. Our theoretical results will be obtained under the usual assumption of $\rho_0 = 0.3\,\mathrm{GeV\,cm^{-3}}$ for the local LSP density. The LSPs are assumed to have a Maxwell-Boltzmann velocity distribution with a characteristic velocity $v_0 = 220\,\mathrm{km/s}$ in the galactic halo, and masses in the region of $m_\chi \approx 100 - 300\,\mathrm{GeV}$ [12–14].

Before discussing our calculations it is worth mentioning that in addition to

the small interaction cross-section with ordinary matter, the WIMPs can annihilate and release various particles (e^+, ν, etc.). The detection of these particles (via indirect CDM-detection experiments) may compete with the direct detection experiments due to the involved large sensitivity to purely axial or spin-dependent couplings. In many cases the indirect detection experiments may be complementary to the direct ones (for more see, e.g. Refs. [2,11]).

2 Brief description of the formalism

In order to access the event rate of the LSP nucleus scattering process one has to start from the differential cross-section $d\sigma(q,v)/dq^2$ where q represents the momentum transfer and v the velocity of the LSP. Instead of q^2 it is convenient to use the dimensionless variable $u = q^2b^2/2$, where b is the nuclear harmonic-oscillator size parameter. Using this notation the differential cross-section in the laboratory frame can be expressed in a compact way as described in detail in [16–18]. This form of the cross section serves as a starting point for the present discussion and it reads

$$\frac{d\sigma(u,v)}{du} = \frac{1}{2}\sigma_0 \left(\frac{1}{m_p b}\right)^2 \frac{v^2}{c^2} \frac{d\sigma_{AS}(u,v)}{du} \tag{1}$$

with

$$\begin{aligned}\frac{d\sigma_{AS}(u,v)}{du} &= \left(f_A^0\Omega_0\right)^2 F_{00}(u) + 2f_A^0 f_A^1 \Omega_0\Omega_1 F_{01}(u) \\ &+ \left(f_A^1\Omega_1\right)^2 F_{11}(u) + A^2\left(f_S^0 - f_S^1\frac{A-2Z}{A}\right)^2 |F(u)|^2\,,\end{aligned} \tag{2}$$

where the values of the nucleonic-current parameters f_A^ρ and f_S^ρ depend on the specific SUSY model employed [16]. Eq. (2) contains all the information about the nuclear structure in the spin structure functions $F_{\rho\rho'}(u)$, $\rho,\rho' = 0,1$, the static spin matrix elements Ω_ρ and the nuclear form factor $F(u)$ [16,18].

One can access the event rate in a CMD detector by selecting a particle-physics model, a halo density distribution and an LSP velocity dispersion $\langle v^2\rangle^{1/2}$. A value commonly adopted for the halo density is $\rho(0) = 0.3$ GeV/cm^3. When considering the event rate R for a detector of mass m_{det} one can write

$$R = \frac{dN}{dt} = \frac{\rho(0)}{m_\chi}\frac{m_{det}}{Am_p} v\sigma(v)\,, \tag{3}$$

where v_z is the LSP velocity relative to the detector and $\sigma(v)$ the total cross section, integrated over the variable u in Eq. (1).

To take into account the participation of the nuclear target in Earth's revolution around the Sun and Sun's motion with respect to the center of our galaxy, one has to fold the above rate with the velocity distribution of the LSP's in the galactic halo. Assuming a Maxwellian velocity distribution one can write

$$f(\mathbf{v}, \mathbf{v}_{\rm E}) = \left(\sqrt{\pi} v_0\right)^{-3} e^{-(\mathbf{v}+\mathbf{v}_{\rm E})^2/v_0^2} , \tag{4}$$

where $v_0 = [(2/3)\,\langle v^2 \rangle]^{1/2} = 220$ km/s, $\mathbf{v}_{\rm E}$ is the velocity of the Earth with respect to the galactic center. Its magnitude depends on $\cos\alpha$), where α is known as the phase of Earth's revolution ($\alpha = 0$ around 2nd of June and $\alpha = \pi$ around 2nd of December).

Making the folding with the distribution of Eq. (4) leads to a folded event rate $\langle R \rangle$ of the form

$$\langle R \rangle = \left\langle \frac{dN}{dt} \right\rangle = \frac{1}{2}\sigma_0 \left(\frac{1}{m_{\rm p} b}\right)^2 \frac{v^2}{c^2} \frac{\rho(0)}{m_\chi} \frac{m_{\rm det}}{A m_{\rm p}} \sqrt{\langle v^2 \rangle}\, \langle \Sigma \rangle , \tag{5}$$

where

$$\langle \Sigma \rangle = \int \frac{|v_z|}{\sqrt{\langle v^2 \rangle}} f(\mathbf{v}, \mathbf{v}_{\rm E}) \sigma_{\rm AS}(|\mathbf{v}|) d^3\mathbf{v} . \tag{6}$$

By taking the polar axis into the direction of $\mathbf{v}_{\rm E}$ and integrating over the angles one finally ends up with

$$\langle R \rangle = \left[\left(f_{\rm A}^0\right)^2 D_1 + 2 f_{\rm A}^0 f_{\rm A}^1 D_2 + \left(f_{\rm A}^1\right)^2 D_3 + A^2 \left(f_{\rm S}^0 - f_{\rm S}^1 \frac{A-2Z}{A}\right)^2 D_4 \right] m_{\rm det} \tag{7}$$

where $m_{\rm det}$ is the detector mass in units of kg. The coefficients D_n contain all the information about the nuclear structure and halo profile and are defined as

$$D_1 = \int_{x_{\rm min}}^{x_{\rm max}} \int_{u_{\rm min}}^{u_{\rm max}} G(x,\lambda) F_{00}(u) \Omega_0^2 du dx , \tag{8}$$

$$D_2 = \int_{x_{\rm min}}^{x_{\rm max}} \int_{u_{\rm min}}^{u_{\rm max}} G(x,\lambda) F_{01}(u) \Omega_0 \Omega_1 du dx , \tag{9}$$

$$D_3 = \int_{x_{\rm min}}^{x_{\rm max}} \int_{u_{\rm min}}^{u_{\rm max}} G(x,\lambda) F_{11}(u) \Omega_1^2 du dx , \tag{10}$$

$$D_4 = \int_{x_{\rm min}}^{x_{\rm max}} \int_{u_{\rm min}}^{u_{\rm max}} G(x,\lambda) |F(u)|^2 du dx . \tag{11}$$

In Eqs. (8)–(11) the modulation function $G(x,\lambda)$ is given by

$$G(x,\lambda) = \left[\frac{8.90\times10^{7}\mathrm{y}^{-1}\mathrm{kg}^{-1}}{(m_{\mathrm{p}}b)^2 A m_\chi[\mathrm{GeV}]}\right]\frac{1}{x}e^{-\frac{x^2}{4\lambda^2}}F_0(x)\sqrt{\frac{3}{2}}\frac{2e^{-\lambda^2}}{\sqrt{6\pi}}\ , \tag{12}$$

with $x = 2\lambda v/v_0$, $\lambda = v_{\mathrm{E}}/v_0$ and v_{E} given below Eq. (4). Here we have defined $F_0(x) = 1 + x\sinh x - \cosh x$. The integration limits are defined as follows

$$x_{\mathrm{min}} = 2\lambda\frac{c}{v_0}\sqrt{\frac{Q_{\mathrm{thr}}}{2\mu_{\mathrm{r}}c^2}}\ , \tag{13}$$

$$x_{\mathrm{max}} = 2\lambda\frac{v_{\mathrm{esc}}}{v_0}\ , \tag{14}$$

$$u_{\mathrm{min}} = \mu_{\mathrm{r}}Q_{\mathrm{thr}}b^2\ , \tag{15}$$

$$u_{\mathrm{max}} = \frac{(\mu_{\mathrm{r}}b)^2}{2\lambda^2}v_0^2x^2\ , \tag{16}$$

where $v_{\mathrm{esc}} = 625$ km/s, Q_{thr} is the detector threshold energy and M_χ is the mass of the LSP. It is worh pointing out that in the work [17] we used an approximation where instead of the above listed exact limits the limits $x_{min} = 0$, $x_{\mathrm{max}} = \infty$ and $u_{\mathrm{min}} = \mu_r Q_{\mathrm{thr}}b^2$, $u_{\mathrm{max}} = 2(v_{\mathrm{esc}}\mu_r b)^2$ were used. Below we will discuss the accuracy of this approximation.

3 Realistic calculations for the LSP-nucleus detection rates

In the present work the nuclear-structure calculations were handled by the shell-model code EICODE [19], a recently created shell-model program that uses proton and neutron basis states projected to good angular momentum. The EICODE uses the same working principles as the shell-model code NATHAN [20] and can handle very large shell-model problems. In the present calculations the states of the nucleus ^{23}Na were easily handled by the EICODE using the USD residual interaction and the single-particle energies quoted in [21]. For the other dark-matter detectors large-scale shell-model calculations had to be performed to access their ground-state wave functions.

For the pf-shell nuclei ^{71}Ga and ^{73}Ge we used the p-f-$g_{9/2}$ model space including the orbitals $1p_{1/2}$, $1p_{3/2}$, $0f_{5/2}$ and $0g_{9/2}$. For the two-body interaction we used an effective G-matrix derived from the CD-Bonn potential using the folded-diagram techniques [22]. For ^{127}I we used the s-d-$g_{9/2}$-$h_{11/2}$ model space including the orbitals $2s_{1/2}$, $1d_{3/2}$, $1d_{5/2}$, $0g_{7/2}$ and $0h_{11/2}$. Also in this case the effective interaction was derived from the CD-Bonn potential [22]. As the single-particle energies we used the ones quoted in [23], choosing $\epsilon(0g_{7/2}) = -0.3$ MeV. These two model spaces have the advantage that they do not produce any spurious center-of-mass admixtures to the calculated wave

functions.

For the nuclei ^{71}Ga and ^{73}Ge we used a configuration truncation method based on configuration energy. In this truncation scheme the average energies of proton and neutron configurations are evaluated prior to the shell-model calculation. Only those configurations which have their average energy below a set threshold are accepted. In this way we have good chances to include the most important many-particle–many-hole configurations in our shell-model wave functions. The convergence of the ground-state energy of ^{73}Ge as a function of the dimension of the truncated Hamiltonian matrix emerging from our energy-based truncation method, is extensively discussed in Ref. [27].

For the nucleus ^{127}I we performed the shell-model calculation using a truncation where at most six neutrons were allowed to be on the $0h_{11/2}$ single-particle orbital. The three valence protons were allowed to have all possible configurations. This truncation resembles the one made in ref. [23] for ^{127}I in the same s-d-$g_{9/2}$-$h_{11/2}$ model space.

Nucleus	$< \mathbf{S_n} >$	$< \mathbf{S_p} >$	$< \mathbf{L_n} >$	$< \mathbf{L_p} >$	$\mu_{\mathrm{exp.}}$	μ_{SM}	$\mu_{\mathrm{s.p.}}$
^{73}Ge	0.4067	0.0048	3.7537	0.3348	-0.879	-1.202	-1.913
^{71}Ga	0.0382	0.3360	0.2810	0.8687	+2.562	+2.691	+3.793
^{23}Na	0.0199	0.2477	0.3207	0.9115	+2.218	+2.220	+3.793
^{127}I	0.0382	0.3299	0.7018	1.4301	+2.813	+3.127	+4.793

Table 1
Comparison of the calculated (μ_{SM}) and measured ($\mu_{\mathrm{exp.}}$) magnetic moments for the discussed nuclei. The single-particle value ($\mu_{\mathrm{s.p.}}$) of the magnetic moment is given to indicate the effect of correlations in the ground-state wave function. The spin and orbital angular-momentum matrix elements for protons and neutrons are also presented.

	^{71}Ga		^{73}Ge		^{127}I		^{23}Na	
	Ω_0	Ω_1	Ω_0	Ω_1	Ω_0	Ω_1	Ω_0	Ω_1
SM	0.905	0.830	0.912	-0.891	0.871	0.690	0.691	0.588
MQPM	0.919	0.925	0.978	-1.070	1.220	1.230	-	-

Table 2
Calculated results for the static spin matrix elements.

For all four detector nuclei we get quite satisfactory ground-state magnetic moments from our truncated shell-model calculations as shown in Table 1. For ^{23}Na the results are practically exact due to the fact that the USD interaction has been fitted to the energies and other observables of several sd-shell nuclei. For the other nuclei the magnetic moments are reasonably close to the corresponding experimental values shown in the table. In particular, the

included correlations in the ground-state wave functions are able to bring the calculated magnetic moments far from their single-particle values (shown in the final column of the table) close to the experimental ones. For completeness, the table also summarizes the calculated ground-state expectation values of spin and orbital angular-momentum operators.

4 Results and Discussion

Our calculated results for the static spin matrix elements are presented in Table 2. These are compared to the ones calculated with the MQPM model of [17]. As can be seen, in the case of ^{71}Ga and ^{73}Ge the two results are quite close to each other, but far apart in the case of ^{127}I. The case of ^{127}I is mainly explained by the fact that in [17] the MQPM model gives a rather pure one-quasiparticle character to the ground state of ^{127}I leading to too large a magnetic moment, close to its single-particle estimate. Thus, it is plausible that the MQPM model also yields too large values for the static spin matrix elements. In the present work the nuclear wave function is more complete and, consequently, the calculated magnetic moment is far from its single-particle value and close to the experimental one. This leads to smaller values of the static spin matrix elements.

The values of the static spin matrix elements can also be compared to results of the previous works. For the case of ^{73}Ge our calculated values are somewhat smaller than the ones of Ref. [24], where $[\Omega_0]^2 = 1.125$, $[\Omega_1]^2 = 1.021$ and $\Omega_0\Omega_1 = -1.072$ were obtained. The larger values of [24] can be partly explained from the fact that by increasing the size of the configuration space the magnitude of the expectation value of the neutron spin-operator decreases [27]. Thus, the value of the static spin matrix element also decreases. The same phenomenon can also be seen in the case of the proton spin operator. However, direct comparison with the results of [24] is complicated by the fact that the interaction used in [24] is not quite the same as the interaction used in the present work. For ^{127}I our results can be compared to the work of Ref. [23]. In this case the two calculations produce practically the same static spin matrix elements.

One of the our main results concerns the computed values of the coefficients $D_1 - D_4$ in Eqs. (8)–(11). They are given in Ref. [27]. Since the values of these coefficients depend on the LSP mass M_χ and the detector threshold energy $Q_{\rm thr}$ it is convenient to express them as a parametrized surface. This enables the reader to use a pocket calculator to extract the values of these coefficients for the wanted LSP mass and detector threshold energy. The parametrization

was done by fitting the computed coefficients by using the function

$$D_n = \frac{e^{-k_1^{(n)} Q_{\rm thr}}}{M_\chi}(k_2^{(n)} + k_3^{(n)} M_\chi + k_4^{(n)} M_\chi^2 + k_5^{(n)} Q_{\rm thr} + k_6^{(n)} M_\chi Q_{\rm thr}), \quad (17)$$

where D_n is given in units of $\mathrm{y}^{-1}\mathrm{kg}^{-1}$ when M_χ is given in units of GeV and $Q_{\rm thr}$ in units of keV. The fitting was done for the ranges of $0\,\mathrm{keV} \leq Q_{\rm thr} \leq 30\,\mathrm{keV}$ and $100\,\mathrm{GeV} \leq M_\chi \leq 300\,\mathrm{GeV}$. Due to the increasing inaccuracy of the fit outside these ranges this parametrization should only be used for the specified ranges. Note that the last two terms are needed only in certain cases.

The coefficient D_n represent the effect of the annual modulation of the event rate. The maximum rate occurs in the 2nd of June and the minimum in the 2nd of December, the difference of these two being connected to the annual modulation amplitude.

To demonstrate the use of the coefficients D_n we take ^{71}Ga as an example. In the case of an ideal detector ($Q_{\rm thr} = 0$) and $M_\chi = 110$ GeV we obtain for the coefficients the calculated annual average values $D_1 = 11.7$, $D_2 = 11.0$, $D_3 = 10.3$, $D_4 = 14.3$ in units of $\mathrm{y}^{-1}\mathrm{kg}^{-1}$. Inserting now into Eq. (7) the parameters of the reader's favourite sypersymmetric model and the active mass of the LSP detector in kilograms one obtains the detected event rate in units of $\mathrm{y}^{-1}\mathrm{kg}^{-1}$.

The error in the fit (17) is less than few per cent for each calculated point. In Table 3 we compare in the case of ^{71}Ga the fitted minimum value of the D_1 coefficient to the calculated one. Like the table shows, the errors of the fit are less than two percent, which is much less than the uncertainties in nuclear-structure calculations. The fitting was done in 16 points, as seen from Table 3.

	100 GeV		150 GeV		200 GeV		300 GeV	
$Q_{\rm thr}$	fit	calc	fit	calc	fit	calc	fit	calc
0.0	10.37	10.41	8.16	8.19	6.79	6.70	4.91	4.89
10.0	8.32	8.31	6.55	6.58	5.45	5.39	3.94	3.94
20.0	6.68	6.61	5.25	5.28	4.37	4.34	3.16	3.18
30.0	5.36	5.26	4.22	4.25	3.51	3.52	2.54	2.59

Table 3
Comparison of the fitted and calculated values of $D_1^{(\rm min)}$ for ^{71}Ga.

In Ref. [17] the folding integral was calculated in an approximative way. The related approximations yield typically an error of a factor 1.5 - 2 to the total event rate. However, the error can be even larger in the case of supersymmetric models which emphasize the role of the spin-dependent channel. The greater

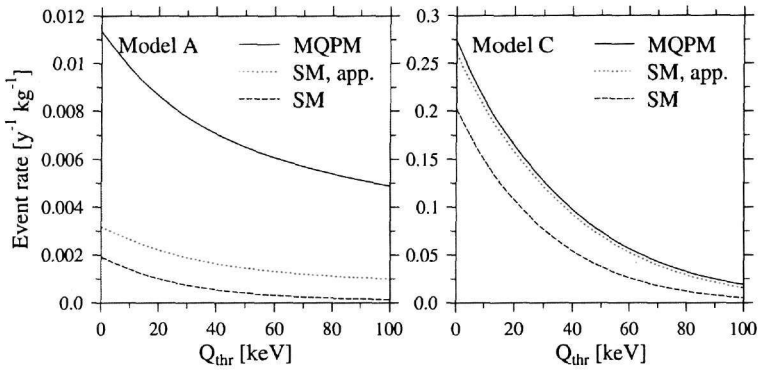

Fig. 1. Calculated event rates in ^{127}I as a function of the detector threshold energy $Q_{\rm thr}$. The used models are the MQPM and the shell model. For the shell-model calculation both the exact folding integrals of Eqs. (8)–(16) and the approximation of Ref. [17] are shown. The supersymmetric model used is the NQM solution 5 of [16] with $M_\chi = 110$ GeV.

sensitivity of the spin-dependent channel, compared to the coherent channel, stems from the fact that the value of the form factor $|F(u)|^2$ is typically smaller than the values of the spin structure functions $F_{\rho\rho'}(u)$ for $u > 0.5-1.0$, depending on the nucleus in question. As a result a relatively bigger part of the spin structure function, compared to the form factor, is left out in the exact folding integration due to its $u_{\rm max}$ limit which depends on the parameter x. In the approximation this limit was extended to infinity and both the form factor and the spin structure functions were included completely.

In Fig. 1 we have plotted the calculated event rates for ^{127}I as a function of the detector threshold energy $Q_{\rm thr}$. We have taken as examples models A and C of the NQM solution 5 [16], the LSP mass being 110 GeV and $\lambda = 1$. The event rate predicted by each of the models has been plotted for three different calculations. The MQPM calculation is based on the approximations to the folding integral introduced in Ref. [17]. In addition, there are two shell-model calculations, one based on the previously mentioned approximations of the folding integral and the other one using the exact folding.

In the case of the supersymmetric model A the event rate stems mainly from the incoherent spin-dependent channel, whereas in the case of model C the event rate is dominated by the coherent channel. From the event rates of model A one can see the drastic effect of the larger values on the static spin matrix elements produced by the MQPM as compared to the SM. Contrary to this, in the case of model C the MQPM and the shell model with the folding approximation give almost the same results. This is due to the fact that these two models produce very similar form factors $|F(u)|^2$. Similarly, in the cases of ^{71}Ga and ^{73}Ge the form factors produced by the two calculations are almost

identical.

In the light of the present experimental situation it is unclear which of the present SUSY models (if any) are the most relevant ones. As mentioned, the event rate (or cross-section) of the LSP scattering can be split into two parts: the coherent and the incoherent one. In this work the incoherent channel is represented by the coefficients $D_{1,2,3}$ and the coherent channel by the coefficient D_4. The different SUSY parametrizations weight differently these two channels and, therefore, can lead to quite different event rates. This has important consequences: if the event rate is dominated by the incoherent channel scattering, like in the case of the NQM solution 5, model A, the experimental setups which use natural germanium are not very sensitive to the WIMP signal, due to the low abundance of the odd-mass isotope ^{73}Ge in natural germanium.

In Ref. [25] the authors examine the possibility to explain the DAMA results [26], contradicting the null results of the other dark-matter experiments, by the dominance of the spin-dependent incoherent channel. The analysis may hint to the importance of the incoherent channel in the LSP-nucleus scattering. This could offer severe limitations to the allowed parameter spaces of supersymmetric models.

As mentioned before, the computed annual minimum and maximum values of the coefficients D_n (see Ref. [27]) describe the annual variation of the observed event rate. In Ref. [27] we do this for the ^{127}I target in the case of the NQM solution 5 and lpot the event rates for three different detector threshold energies $Q_{\rm thr}$. To a good approximation, the event rates have a sinusoidal form, so that the modulation pattern can be deduced easily from the minimum and maximum values of the event rates which deviate about 15% from the annual average value. Many of the present experimental setups aim at observing this annual modulation.

5 Summary and conclusion

We have calculated the expected LSP-nucleus elastic scattering event rates for the promising CDM detectors ^{23}Na, ^{71}Ga, ^{73}Ge and ^{127}I. The calculation of the wave functions of the involved ground states of these nuclei were done in the shell-model framework using realistic single-particle spaces and effective microscopic two-body interactions. Large-scale shell-model computations had to be done in order to achieve convergence of the results. The adequacy of the nuclear-strucrure ingredients was tested by comparing the computed magnetic moments of these states with data. The computed observables of the LSP-nucleus scattering were compared with earlier calculations and our previous

work where approximations both in nuclear structure and even-rate folding were done.

To enable studies of different SUSY parametrizations we have worked out a representation of the LSP-nucleus scattering problem where the nuclear-structure aspects have been separated from the particle-physics aspects. By parametrizing the nuclear-structure part in terms of the LSP mass and the detector threshold we have produced a table applicable to any SUSY scenario. These tables are easily used to survey the parameter spaces of SUSY models, say, to study which models yield detectable event rates in detectors of a given fiducial mass.

We have also addressed the detection rates and the annual modulation signal in the four studied CDM detectors. To see the differences in the nuclear inputs we have compared two nuclear models, the MQPM and the nuclear shell model, in computation of the event rates. We have found that the form factors, relevant in the coherent-channel scattering, are quite independent of the used nuclear model. In the case of the spin-dependent incoherent channel the two used nuclear models gave notably different results, especially in the case of ^{127}I. We have found that the different SUSY scenarios weight the spin-dependent channel in quite different ways. This opens a way to speculations about the claimed detection of the annual modulation signal by the DAMA experiment. A SUSY scenario favouring estreme spin-dependence could explain the DAMA signal and the non-observation of the signal in the other experiments where even nuclei are used as detectors leading to domination of the coherent channel.

Acknowledgements:

This work has been partially supported by the IKYDA-02 project and by the Academy of Finland under the Finnish Centre of Excellence Programme 2000-2005 (Project No. 44875, Nuclear and Condensed Matter Programme at JYFL).

References

[1] G. Jungman, M. Kamionkowski, K. Griest, Phys. Rep. 267 (1996) 195.

[2] G. Bertone, D. Hooper, J. Silk, Phys. Rep. 405 (2005) 279, and references therein.

[3] J.D. Vergados, Phys. Rev. Lett. 83 (1999) 3597; Phys. Rev. D 62 (2000) 023519; Phys. Rev. D 67 (2003) 103003.

[4] R. Bernabei, et al., Phys. Lett. B 480 (2000) 23; Abusaidi, et al., Phys. Rev. Lett. 84 (2000) 5699.

[5] D.S. Akerib and the CDMS Collaboration, Phys. Rev. D 68 (2003) 082002; astro-ph/0405033.

[6] A. Benoit and the EDELWEISS Collaboration, Phys Lett. B 545 (2002) 43.

[7] G. Angloher, et al., Astropart. Phys. 18 (2002) 43; M. Bravin, et al., Astropart. Phys. 12 (1999) 107.

[8] S. Cebrian, et al., astro-ph/0112272.

[9] N.J.T. Smith, et al., The Identification of Dark Matter, Eds. N.J.C. Spooner and V. Kudryavtsev (World Scientific, 1999), p. 335.

[10] R. Bernabei, et al., Phys. Lett. B 509 (2001) 197; Nucl. Phys. (Proc. Suppl.) B 110 (2002) 61; Eur. Phys. J. C 23 (2002) 61.

[11] R. Bernabei, et al., astro-ph/0501412, and references therein.

[12] M.E. Gomez, J.D. Vergados, Phys. Lett. B 512 (2001) 252; M. Gomez, G. Lazarides, C. Pallis, Phys. Lett. B 487 (2000) 313; Phys. Rev. D 61 (2000) 123512.

[13] P. Nath, R. Arnowitt, Phys. Rev. D 39 (1989) 279; *ibid* D 56 (1997) 2820; R. Arnowitt, B. Dutta, Supersymmetry and Dark Matter, hep-ph/0204187.

[14] A. Bottino, et al., Phys. Lett. B 265 (1991) 57; Phys. Lett. B 402 (1997) 113.

[15] J.D. Vergados, H. Ejiri, Phys Lett. B 606 (2005) 313.

[16] J.D. Vergados, J. Phys G 22 (1996) 253; J.D. Vergados, T.S. Kosmas, Phys. At. Nucl. 61 (1998) 1166.

[17] E. Holmlund, M. Kortelainen, T.S. Kosmas, J. Suhonen, J. Toivanen, Phys Lett. B 584 (2004) 31.

[18] P.C. Divari, T.S. Kosmas, J.D. Vergados, L.D. Skouras, Phys. Rev. C 61 (2000) 054612.

[19] J. Toivanen, computer code EICODE, JYFL, Finland (2004).

[20] E. Caurier, et al., Phys. Rev. C 59 (1999) 2033.

[21] B.H. Wildenthal, Prog. Part. Nucl. Phys. 11 (1984) 5

[22] M. Hjorth-Jensen, T.T.S. Kuo, E. Osnes, Phys. Rep. 260 (1995) 125; M. Hjorth-Jensen, private communication.

[23] M.T. Ressel, D.J. Dean, Phys. Rev. C 56 (1997) 535.

[24] M.T. Ressel, et al., Phys. Rev. D 48 (1993) 5519.

[25] C. Savage, P. Gondolo, K. Freese, Phys. Rev. D 70 (2004) 123513.

[26] R. Bernabei, et al., astro-ph/0405282.

[27] M. Kortelainen, T.S. Kosmas, J. Suhonen, J. Toivanen, Phys Lett. B, in press.